



Cite this: *CrystEngComm*, 2019, 21, 7322

A new phosphotungstate-supported rhenium carbonyl derivative: synthesis, characterization and catalytic selective oxidation of thiophenes†

Jingkun Lu, Junwei Feng, Xinyi Ma, Ping Wang, Baijie Xu, Peipei He, Jiage Jia, Pengtao Ma,  Jingyang Niu * and Jingping Wang *

A monomeric phosphotungstate-supported rhenium carbonyl derivative, $[\text{N}(\text{CH}_3)_4]_6\text{H}_4[\text{P}_2\text{W}_{17}\text{O}_{62}\{\text{Re}(\text{CO})_3\}_2] \cdot 25\text{H}_2\text{O}$ (**1**), has been synthesized in a conventional solution system and structurally characterized by single crystal X-ray diffraction crystallography, IR spectroscopy, thermogravimetric (TG) analyses, X-ray powder diffraction (XRPD), and electrospray ionization mass spectrometry (ESI-MS). To our knowledge, this is the first time that the $\{\text{Re}_2\}$ fragment existing in the polyoxoanion has been observed in polyoxometalate-supported metal carbonyl derivatives. Moreover, UV-vis spectroscopy was employed to elucidate the stability of the polyoxoanion, and its electrochemical properties were also investigated. In particular, complex **1** could act as an efficient homogeneous catalyst for selective oxidation of thiophenes. For example, dibenzothiophene (DBT) undergoes up to 99% conversion and 99% sulfone selectivity in acetonitrile with 30% H_2O_2 as an oxidant.

Received 19th July 2019,
Accepted 24th October 2019

DOI: 10.1039/c9ce01124b

rsc.li/crystengcomm

Introduction

Polyoxometalates (POMs) are a unique family of discrete metal-clusters and have stimulated research in broad fields of science.¹ In particular, considerable attention has been directed toward POM-based organometallic derivatives not only because of their intriguing structural diversity, but also due to their potential catalytic properties.² As a peculiar class of organometallic oxides, POM-based carbonyl metal derivatives are able to provide dual advantages of both a carbonyl fragment and a metal-oxo anionic scaffold, leading to the formation of a number of diverse functional compounds. A series of these compounds with their synthetic routes, stability aspects, and catalytic properties has been widely investigated previously.³ In particular, the carbonyl manganese/rhenium derivatives of POMs with rich behaviors displayed by the d^6 carbonyl metal compounds and the POMs are especially important. However, POM-based carbonyl manganese/rhenium derivatives are

relatively less investigated, mainly because polyoxoanions do not have enough charge density for facile reactivity of metal carbonyl groups, along with their insolubility in most solvents, their radiation or thermal instability and the expensive prices of carbonyl metal salts. Because of the synthetic intricacies mentioned above, most of the known POM-based carbonyl manganese/rhenium compounds are dominated by Lindqvist-type POMs.⁴ From 2008, our group has reported the preparation and structural characterization of a series of POM-based carbonyl manganese/rhenium derivatives, such as $[\{\text{H}_2\text{W}_8\text{O}_{30}\}\{\text{M}(\text{CO})_3\}_2]^{8-}$ ($\text{M} = \text{Mn}^{\text{I}}$ and Re^{I}),^{5a} $[\{\text{H}_2\text{Mo}_8\text{O}_{30}\}\{\text{M}(\text{CO})_3\}_2]^{8-}$ ($\text{M} = \text{Mn}^{\text{I}}$ and Re^{I}),^{5b} $[\{\text{PMo}_3\text{O}_{16}\}\{\text{Re}(\text{CO})_3\}_4]^{5-}$,^{5c} $[\{\text{PW}_{11}\text{O}_{39}\}\{\text{Re}(\text{CO})_3\}_3(\mu_3\text{-O})(\mu_2\text{-OH})]^{7-}$,^{5d} $[\{\text{Re}(\text{CO})_3\}_4(\mu_2\text{-OH})(\mu_3\text{-O})(\text{W}_5\text{O}_{18})]^{5-}$,^{2f} $[\text{P}_2\text{W}_{15}\text{O}_{56}\text{Co}_3(\text{H}_2\text{O})_3(\text{OH})_3\text{Mn}(\text{CO})_3]^{8-}$,^{2e} $[\{\text{Re}(\text{CO})_3\}_4(\text{Mo}_4\text{O}_{16})]^{4-}$,^{2d} $[\{\text{Mn}(\text{CO})_3\}_4(\text{Se}_2\text{W}_{11}\text{O}_{43})]^{8-}$,^{5e} $[\text{Te}_2\text{W}_{20}\text{O}_{70}\{\text{Re}(\text{CO})_3\}_2]^{10-}$,^{5f} *etc.* As a continuation of our recent research on the synthesis and catalytic application of novel POM-based carbonyl rhenium derivatives, considerable attention has been directed towards these compounds, due to their novel structures and attractive catalytic properties.

Organic sulfur compounds present in fuels have aroused worldwide concern because they can cause a series of environmental problems, such as acid rain and haze.⁶ Thus, many countries have promulgated regulations and policies to control the sulfur content in fuels. Various desulfurization technologies have been widely investigated such as hydrodesulfurization (HDS), extraction desulfurization (EDS), biodesulfurization and oxidative desulfurization (ODS). HDS is the conventional technology in modern industry,⁷ but ODS

Henan Key Laboratory of Polyoxometalate Chemistry, Institute of Molecular and Crystal Engineering, College of Chemistry and Chemical Engineering, Henan University, Kaifeng, Henan 475004, P. R. China. E-mail: jyniu@henu.edu.cn, jpwang@henu.edu.cn; Fax: (+86)371 23886876

† Electronic supplementary information (ESI) available: The bond valence sum calculations (Tables S1 and S2); selected bond lengths and angles (Table S3); additional structural figures (Fig. S1–S3); IR, XRPD, TG and UV-vis spectra (Fig. S4–S10); catalytic properties (Tables S4 and S5, Fig. S11–S15). CCDC: 1939767. For ESI and crystallographic data in CIF or other electronic format see DOI: 10.1039/c9ce01124b

is considered as one of the most promising methods because it can operate efficiently in moderate reaction environments, especially for the removal of aromatic sulfurs, such as benzothiophene (BT) and dibenzothiophene (DBT) derivatives, which are hard to remove by HDS.⁸ POMs have been demonstrated to be active catalysts for ODS processes; for example, various Keggin-type POMs reported by Balula *et al.* were used to desulfurize model and real diesel.⁹

In this work, we have obtained a new phosphotungstate-supported rhenium carbonyl derivative, $[\text{N}(\text{CH}_3)_4]_6\text{H}_4[\text{P}_2\text{W}_{17}\text{O}_{62}\{\text{Re}(\text{CO})_3\}_2]\cdot 25\text{H}_2\text{O}$ (**1**). To the best of our knowledge, compound **1** is the first example to contain a novel $\{\text{Re}_2\}$ unit. Furthermore, the catalysis on **1** for the selective oxidation of DBT in the presence of a hydrogen peroxide (30% H_2O_2) oxidant was studied.

Experimental

General methods and materials

All the chemicals and solvents were purchased from commercial suppliers as reagent grade and used as received without further purification. $\text{Na}_{12}[(\alpha\text{-P}_2\text{W}_{15}\text{O}_{56})]\cdot 24\text{H}_2\text{O}$ was synthesized as previously described.¹⁰ Elemental analysis for C, H and N was performed using a Perkin-Elmer 2400-II CHNS/O analyzer. Thermogravimetric analysis (TGA) was carried out on a Mettler Toledo TGA/SDTA 851° instrument. The heating rate employed was 10 °C min^{-1} under a N_2 atmosphere over a temperature range of 25–700 °C. Fourier transform infrared (FT-IR) spectra were recorded with a Bruker VERTEX 70 IR spectrometer (using KBr pellets) in the range of 4000–450 cm^{-1} . Single-crystal X-ray diffraction measurements were carried out with a Bruker SMART Apex II CCD-based diffractometer at 293 K. UV-vis absorption spectra were obtained using a U-4100 spectrometer, in which the samples were measured in a quartz cuvette with a path length of 1 cm at room temperature. Electrochemical measurements were performed with a three-electrode CV cell, using a CHI660 electrochemical workstation. The working electrode was a freshly cleaned glassy carbon disk electrode, the counter electrode was a platinum wire, and the saturated calomel electrode (SCE) was used as a reference electrode. GC chromatograms were measured on a Bruker 450-GC (FID) instrument, which was equipped with a 30 m column (GsBP-5, 0.25 μm film thickness and 0.25 mm internal diameter) with nitrogen as a carrier gas.

Synthesis of $[\text{N}(\text{CH}_3)_4]_6\text{H}_4[\text{P}_2\text{W}_{17}\text{O}_{62}\{\text{Re}(\text{CO})_3\}_2]\cdot 25\text{H}_2\text{O}$ (**1**)

A sample of $\text{Re}(\text{CO})_5\text{Cl}$ (0.0362 g, 0.1 mmol) was dissolved in 3 mL of CH_3CN , and then refluxed for 30 min at 70 °C (solution 1). $\text{Na}_{12}[\text{P}_2\text{W}_{15}\text{O}_{56}]\cdot 18\text{H}_2\text{O}$ (0.22 g, 0.051 mmol) and lithium acetate (0.02 g, 0.303 mmol) were dissolved in 15 mL distilled water, and stirred at room temperature. The pH of the resulting solution was adjusted to 4.5 with a 50% acetic acid solution (solution 2). After that, solution 1 was added to solution 2, and the mixture was heated at 80 °C and stirred for 1 h. Then, 1 mL of $(\text{CH}_3)_4\text{NCl}$ (1 M) was added and the

solution was stirred for further 10 min, cooled to room temperature and filtered. After slow evaporation for about one week, red crystals suitable for X-ray diffraction were obtained. Yield: 0.12 g (11.79%) for **1** based on $\text{Re}(\text{CO})_5\text{Cl}$. Elemental analysis (%) calcd: C, 6.41; H, 2.26; N, 1.50. Found: C, 7.05; H, 2.35; N, 1.62. IR (KBr, cm^{-1}): 3432 (w), 2011 (vs), 1883 (vs), 1633 (s), 1485 (s), 1087 (s), 1024 (w), 947 (s), 909 (w), 801 (s), 738 (w), 520 (w).

Typical procedure for the oxidation of thiophenes

Typical oxidation reactions of various thiophenes with hydrogen peroxide as model reactions were performed using a 50 ml round-bottom tube equipped with a reflux condenser. The catalytic oxidation reactions were studied as follows: a mixture of substrate (1 mmol), catalyst (the ratio of substrate/catalyst = 200, 300, 500 or 1000), H_2O_2 (1.0 mmol, H_2O_2 /substrate (O/S) = 1; 2.0 mmol, O/S = 2; 3.0 mmol, O/S = 3), and 3.0 mL of CH_3CN was added to the tube at the required temperature. Then, the reaction mixture was stirred (800 rpm) for the requisite time at atmospheric pressure. At regular intervals, gas chromatography (GC) analysis was performed on an aliquot of the reaction mixture using toluene (1 mmol) as the internal standard.

X-ray crystallography

Suitable single crystals (0.25 mm \times 0.22 mm \times 0.20 mm) were selected from the mother liquors and stuck on a glass fiber. Intensity data for **1** were recorded at 296(2) K on a Bruker APEX-II CCD diffractometer with graphite-monochromated Mo $K\alpha$ radiation ($\lambda = 0.71073$ Å). The absorption correction was based on multiple and symmetry equivalent reflections in the data set using the SADABS program. Using Olex2,¹¹ the structure was solved by direct methods with the SHELXS-1997 structure solution program and refined with the SHELXL refinement package using full-matrix least-squares methods.¹² Positions of the hydrogen atoms attached to the carbon and nitrogen atoms were geometrically placed. No hydrogen atoms associated with the water molecules were located from the difference Fourier map. In the final refinement, the P, W, and Re atoms were refined anisotropically. Furthermore, the combination of elemental analysis and thermogravimetric analysis confirmed the number of water molecules of crystallization in the polyoxoanions. All H atoms on the water molecules were directly included in the molecular formula. A summary of the crystal data and structure refinements is listed in Table 1.

Results and discussion

Description of the crystal structure

In 2013, Hill *et al.* reported a similar structure, $[\text{P}_2\text{W}_{17}\text{O}_{61}\{\text{Re}(\text{CO})_3\}_3\{\text{ORb}(\text{H}_2\text{O})\}\{\mu_3\text{-OH}\}]^{9-}$, which was prepared by the reaction of a POM precursor, $[\text{P}_4\text{W}_{35}\text{O}_{124}\{\text{Re}(\text{CO})_3\}_2]^{16-}$, and $[\text{Re}(\text{CO})_3]^+$ complexes in a slightly acidic aqueous solution.^{2h} Compound **1** was also synthesized from an acidified mixture of $\text{Re}(\text{CO})_5\text{Cl}$, $\text{Na}_{12}[\text{P}_2\text{W}_{15}\text{O}_{56}]\cdot 18\text{H}_2\text{O}$, and lithium acetate.

Table 1 Crystal structure data for compound **1**

Formula	$C_{30}H_{126}N_6O_{93}P_2W_{17}Re_2$
M_r (g mol ⁻¹)	5618.9476
Crystal system	Orthorhombic
Space group	<i>Pnma</i>
<i>a</i> (Å)	28.1534(16)
<i>b</i> (Å)	13.4987(8)
<i>c</i> (Å)	31.1648(19)
<i>V</i> (Å ³)	11 843.7(12)
<i>Z</i>	4
Dc (g cm ⁻³)	2.966
μ (mm ⁻¹)	18.581
<i>F</i> (000)	9372.0
2θ range (deg)	3.174 to 50.198
Reflections collected	60 380
Index ranges	$-29 \leq h \leq 33$, $-16 \leq k \leq 16$, $-35 \leq l \leq 37$
Data/restraints/parameters	11 004/54/352
GOF on F^2	1.086
R_1 , wR_2 [$I \geq 2\sigma(I)$]	$R_1 = 0.0606$, $wR_2 = 0.1273$
R_1 , wR_2 [all data]	$R_1 = 0.1000$, $wR_2 = 0.1463$

Complex **1** crystallizes in the orthorhombic space group *Pnma* and consists of a discrete cluster anion $[P_2W_{17}O_{62}\{Re(CO)_3\}_2]^{10-}$ (**1a**), six $[(CH_3)_4N]^+$ cations, four H^+ , and twenty five lattice water molecules. This new polyoxoanion **1a** can be described as grafting two carbonyl rhenium groups $\{Re(CO)_3\}^+$ onto the $\{P_2W_{17}O_{61}\}^{10-}$ ligand in an “out-of-pocket” structural motif (Fig. 1a and b). The organometallic fragments $\{Re(CO)_3\}^+$ are bonded to four adjacent axial oxygen atoms of the $\{P_2W_{17}O_{61}\}^{10-}$ framework and then achieve 18-electron configurations (Fig. S1†). As previously reported, the bonding of the $\{M(CO)_3\}^+$ fragment

($M = Mn$ or Re), in a general way for d^6 -*fac*- ML_3 moieties, to a triangle of bridging oxygen atoms is usually the rule within POM-supported organometallic complexes, and such a coordination mode is also appropriate for compound **1**. Furthermore, the $\{P_2W_{17}O_{61}\}^{10-}$ unit originates from the isomerization of the $\{P_2W_{15}O_{56}\}^{12-}$ skeleton in the starting material $Na_{12}[P_2W_{15}O_{56}] \cdot 18H_2O$. In **1a**, all P atoms adopt a four-coordinated mode and all W atoms are six-coordinated with the usual octahedral geometry. Moreover, four $\{W_2O_{10}\}$ subunits are connected by atom P1, and atom P2 is the center of the trivacant B- α Keggin $\{PW_9O_{33}\}$ unit (Fig. 1c and d). Interestingly, two $\{Re(CO)_3\}^+$ pendants are linked together *via* bridging atom O37, and the bonding mode of the $\{Re_2\}$ moiety is observed for the first time for POM-supported carbonyl metal derivatives. As shown in Fig. 2a, the angle of $Re1-O37-Re1$ is $145.9(4)^\circ$, and atom Re1 is bonded to atom O37 which forms two $Re-O-W$ bonds to the $\{P_2W_{17}O_{61}\}^{10-}$ moiety. Both Re centers exhibit a distorted octahedral ReC_3O_3 coordination defined by three oxygen atoms (O15, O19, and O37) and three carbon atoms from carbonyl groups (C1, C2, and C3) (Fig. 2b). All the $Re-C$ and $Re-O$ bond lengths are in the ranges of $1.76(3)$ – $1.83(4)$ Å and $2.113(13)$ – $2.155(7)$ Å, respectively. The differences between the $Re-C$ bond lengths lie within experimental errors, and it is the same for the three $Re-O$ bond lengths. Bond valence sum (BVS) calculations indicate that all the P atoms and W atoms are in the +5 and +6 oxidation states (Table S1†).¹³ BVS results of all the oxygen atoms indicate that their oxidation states are –2, except for the O37 atom with a BVS value of 1.214, also indicating that O37 may be monoprotated (Table S2†).

IR, XRPD and TGA analyses

IR spectroscopy can provide helpful information for the analysis of POM-based carbonyl metal derivatives. The IR spectrum between 4000 and 450 cm^{-1} is characteristic for the structural framework of **1**. As shown in Fig. S4†, the peaks at 947 , 909 , 801 and 738 cm^{-1} are attributed to the $\nu_{as}(O_b-W-O_b)$ and $\nu_{as}(W-O_c)$ bands, respectively.¹⁴ The signal appearing in the region of 1087 and 1024 cm^{-1} could be ascribed to the characteristic peaks of the P–O vibrations. The resonances at 3432 and 1633 cm^{-1} correspond to the stretching and flexural vibrations of –OH and –NH, while a peak at 1485 cm^{-1} is associated with the flexural vibrations of –CH, confirming the existence of water molecules and $(CH_3)_4N^+$. The characteristic bands at 2011 and 1883 cm^{-1} can be regarded

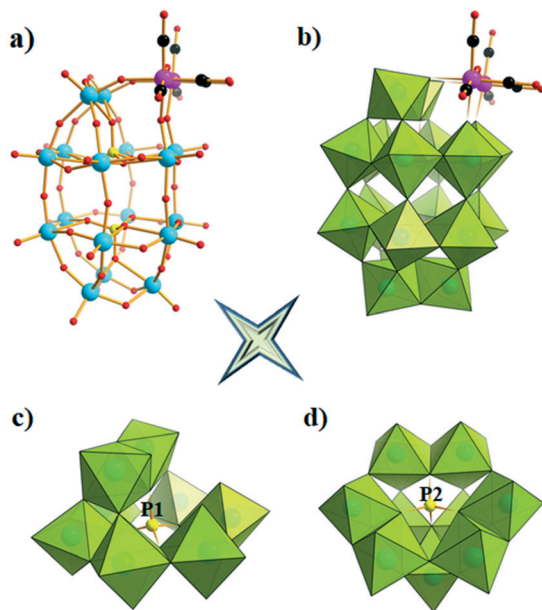


Fig. 1 Combined polyhedral/ball-and-stick representation of polyoxoanion $[P_2W_{17}O_{62}\{Re(CO)_3\}_2]^{10-}$ (a and b). (c) Polyhedral representation of the $\{PW_8\}$ unit. (d) Polyhedral representation of the $\{PW_9\}$ unit. Color code: P, yellow; W, blue; Re, pink; C, black; O, red; WO_6 , light green.

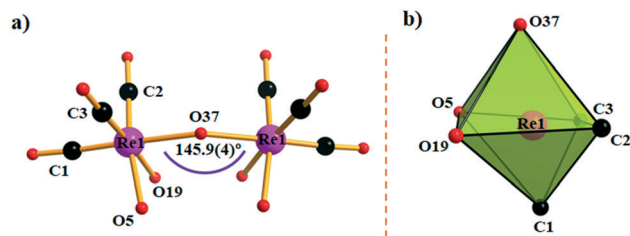


Fig. 2 (a) Ball-and-stick representation of the $[Re_2(CO)_6]$ moiety. (b) The coordination environment of the Re atom. Color code: Re, pink; C, black; O, red; ReC_3O_3 , light green.

as features of the symmetric and antisymmetric stretching vibrations of the C–O bond,¹⁵ respectively. Comparing the IR spectra of Na₁₂[P₂W₁₅O₅₆] \cdot 18H₂O and compound **1** (Fig. S4 and S5), the peaks display obvious splitting and a red shift, which may be attributed to the combination of carbonyl metal groups with POM frameworks. In addition, to indicate the phase purity of compound **1**, XRPD experiments were carried out. The purity of the phase has been checked by comparing the experimental X-ray powder pattern with the powder pattern calculated from the structure solved from the single-crystal X-ray diffraction data. In key positions, the peaks in the experimental spectrum match with those in the simulated one, indicating its crystalline phase purity, and the difference in the intensities of some diffraction peaks may be attributed to the preferred orientation of the crystalline powder sample (Fig. S7[†]).

Thermogravimetric experiments were conducted to study the thermal stability of compound **1** (Fig. S8[†]). The TGA curve of **1** shows a total weight loss of 19.70% (calcd. 18.92%) from 25–800 °C. The first weight loss of 7.94% (calcd. 8.01%) in the range of 25–300 °C corresponds to the release of 25 lattice water molecules. The second weight loss of 11.76% from 300–800 °C is attributed to the release of four protons (in the form of constitutional water molecules), six tetramethylammonium cations and six CO (in the form of CO₂ molecules).

UV-vis spectroscopy and electrochemistry

The electronic properties and the solution stability of compound **1** were studied by cyclic voltammetry (CV) and UV-vis absorption spectroscopy, respectively. As shown in Fig. S9[†], the absorption value at 275 nm is characteristic of the oxygen–tungsten charge-transfer band of POM. In order to investigate the stability of the solution of **1**, *in situ* spectroscopic measurements were performed on the aqueous system. The UV-vis spectra of **1** in aqueous solution (5×10^{-5} mol L⁻¹) with the mixed solvent CH₃CN–H₂O (1:3, volume ratio) displayed a little change over a period of 8 h at room temperature in the dark (Fig. S10[†]). The electrochemical behavior of **1** was studied in 0.4 M CH₃CN/Na₂SO₄ (1:3, volume ratio) electrolyte solutions with different scan rates (Fig. 3). The potential domain of the voltammogram is divided into a positive and a negative section (*vs.* SCE) for its sequential analysis. It can be clearly seen that the redox peaks of W^{VI} centers appear at a more negative potential region than that assigned to the Re^I centers, as expected. In the negative potential domain, two separated quasi-reversible waves at –0.42 V/–0.435 V (I/I') and –0.592 V/–0.629 V (II/II') and one irreversible wave at –0.875 V (III') are respectively assigned to the oxidation/reduction of W^{VI} centers. In the positive potential direction, the irreversible wave at 1.079 V (IV) is associated with the redox process of the [Re(CO)₃]⁺ pendant. With increasing scan rate, the corresponding cathodic and anodic peak intensities slightly increase, but the mean peak potential does not change distinctly. Below 200 mV s⁻¹, the peak current intensity of **1** is proportional to

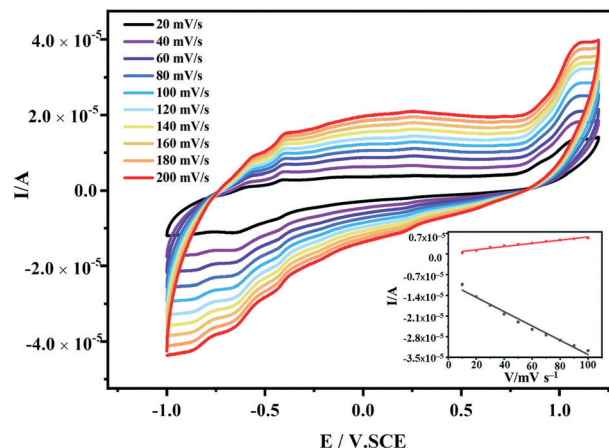


Fig. 3 Cyclic voltammograms of **1** at different scan rates: from inside to outside: 20, 40, 60, 80, 100, 120, 140, 160, 180, and 200 mV s⁻¹. Inset: Representation of the current as a function of the scan rate.

the scan rate, demonstrating that the redox process becomes diffusion-controlled, and similar behaviours were observed in the case of other compounds.^{5f,16}

Electrospray ionization mass spectrometry (ESI-MS) analysis

It is worth pointing out that ESI-MS studies have been extremely helpful in an effort to identify the composition and the degree of protonation, as well as investigating the existence of other relatively stable species in the solution.¹⁷ Herein, ESI-MS was used to determine the number of products present and their distribution. Single crystals of **1** were dissolved in CH₃CN and transferred into the gas phase by electrospray ionization (ESI). The formulas for the anions observed were confirmed by the experimental values of *m/z* as well as the isotopic profile. Critical analysis permitted us to accurately assign envelopes of charged species, namely –4. The ESI-MS result shows that there were four peaks located at *m/z* 1194.88, 1213.39, 1217.34 and 1236.43 which belong to [P₂W₁₇O₆₂{Re(CO)₃}₂H₆(H₂O)₃]⁴⁻ (calc.

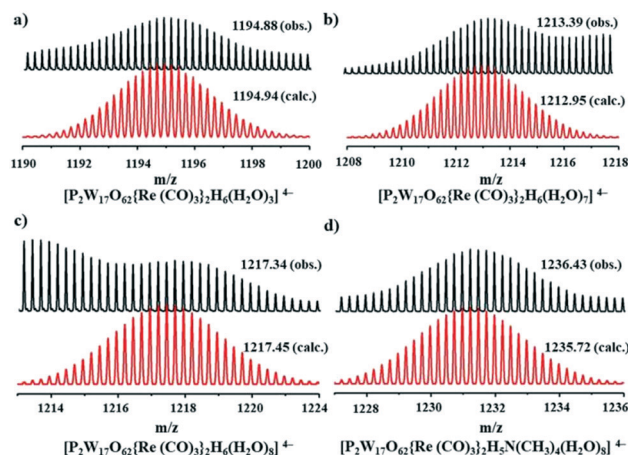


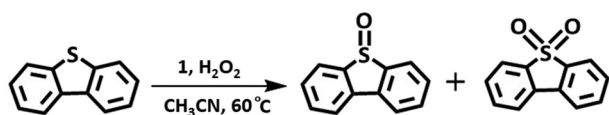
Fig. 4 Negative-ion ESI-MS mass spectra of **1a** in CH₃CN (calculated spectra in red; actual spectra in black).

Table 2 Effect of reaction parameters on the oxidation reaction of DBT catalyzed by **1**^a

Entry	S/C molar ratio	H ₂ O ₂ ^b	Temp. (°C)	Solvent	Con. ^c (%)	Sel. ^d (%)
1 ^e	—	3	60	CH ₃ CN	6.7	99
2	200	3	60	CH ₃ CN	99	99
3	300	3	60	CH ₃ CN	88	92
4	500	3	60	CH ₃ CN	73	90
5	1000	3	60	CH ₃ CN	55.9	90
6	200	3	55	CH ₃ CN	48	99
7	200	3	45	CH ₃ CN	19	100
8	200	2	60	CH ₃ CN	83	86
9	200	1	60	CH ₃ CN	21	69
10	200	3	60	H ₂ O	8.1	60
11	200	3	60	CH ₃ CH ₂ OH	16	73
12	200	3	60	CCl ₄	20	54

^a Reaction conditions: catalyst, substrate (1 mmol), internal standard (toluene, 1 mmol) and 30% H₂O₂ were mixed in 3 mL solvent, 1 h.

^b H₂O₂/substrate molar ratio. ^c Conversions were determined by GC-FID. ^d Selectivity to sulfone. ^e Blank experiment.

**Scheme 1** Catalytic oxidation of dibenzothiophene (DBT).

1194.94), [P₂W₁₇O₆₂{Re(CO)₃}₂H₆(H₂O)₇]⁴⁻ (calc. 1212.95), [P₂W₁₇O₆₂{Re(CO)₃}₂H₆(H₂O)₈]⁴⁻ (calc. 1217.45), and [P₂W₁₇O₆₂{Re(CO)₃}₂H₅N(CH₃)₄(H₂O)₈]⁴⁻ (calc. 1235.72), respectively (Fig. 4). Thus, these experiments provide definitive proof for the presence of intact clusters in solution.

Catalytic properties

Optimization of the catalyst. Sulfoxidation catalysis using H₂O₂ as an oxidant under mild conditions is considered one of the most promising reactions in industrial chemistry.¹⁸ In this study, the influence of different reaction parameters on the efficiency of the oxidation process was evaluated in the model

reaction showed in Table 2. Here, DBT was used as the benchmark substrate to study the catalytic oxidation of thiophene in the presence of **1** in acetonitrile, which showed 99% conversion for and 99% selectivity to its corresponding sulfone (Table 2, entry 2). Besides, the raw materials, Na₁₂[P₂W₁₅O₅₆].18H₂O, Re(CO)₅Cl, and CH₃COOLi, showed somewhat low catalytic activity compared with catalyst **1** (Table S4†). A blank reaction (without any catalyst) was investigated for DBT, confirming that less oxidation occurred in the absence of the catalyst (6.7% conversion for DBT; Table 2, entry 1). The yield was significantly increased by adding the catalyst, and as expected, the use of a higher amount of catalyst **1** (S/C molar ratio = 200) afforded the best results for DBT. Moreover, increasing the reaction temperature accelerates the process of DBT oxidation, as listed in Table 2, entries 6–7. We found that a higher reaction temperature leads to acceleration of the DBT oxidation. A lower temperature, however, is disadvantageous for the oxidation reaction and the conversion is less than 20% at 45 °C. Therefore, a reaction temperature of 60 °C was chosen for the further improvement of the reaction conditions (Scheme 1).

Table 3 Sulfoxidation with different substrates with H₂O₂ catalyzed by **1**^a

Substrate	S/C molar ratio	Time (h)	Product	Con. ^b (%)	Sel. (%)
	200	1.0		99	99
	1000	1.5		96	97
	200	1.5		95	93
	1000	2.0		92	91
	200	1.0		92	100
	1000	1.5		89	98
	200	1.0		99	96
	1000	1.5		98	95

^a Reaction conditions: the substrate (1.0 mmol), the catalyst corresponding to the substrate/catalyst (S/C) molar ratios of 200 and 1000, the internal standard (toluene, 1 mmol) and 30% H₂O₂ (3.0 mmol) were stirred in 3.0 mL of CH₃CN at 60 °C. ^b Conversions were determined by GC-FID.

In addition, we have screened different H₂O₂/substrate (O/S) molar ratios for the oxidation of DBT. When the O/S molar ratio was varied from 1:1 to 2:1 to 3:1, the degree of selectivity varied from 69% to 86% to 99%, respectively (entries 2, 8 and 9). Based on these results, the O/S molar ratio of 3:1 was used for the following studies. As previously reported, the solvent plays an important role in determining the catalytic activity and selectivity in many catalytic oxidation reactions with H₂O₂.¹⁹ Then, we investigated the oxidation of DBT in different solvents, and the results showed that the reaction is sensitive to the solvent. For example, using H₂O, CH₃CH₂OH, and CCl₄ as solvents, the conversions are 8.1%, 16% and 20%, respectively, and the selectivities toward sulfones are all less than 80%, which may be due to the low solubility of the catalyst in these solvents (entries 10–12). CH₃CN turned out to be the best solvent providing the highest conversion (99%) and the best selectivity (99%).

Sulfoxidation with different substrates. Having established the optimized reaction conditions for selective oxidation of the model substrate, we extended the study to the other thiophenic compounds BT (benzothiophene), 3-MBT (3-methylbenzothiophene), and 4-MDBT (4-methyldibenzothiophene), the results of which are summarized in Table 3. The reaction shows satisfactory general applicability for the production of sulfones. Generally, the oxidation reactivity decreased in the order DBT > BT, which is attributed to the significantly lower electron density on the sulfur atom of BT (the electron densities on the sulphur atoms are reported to be 5.739 and 5.758 for BT and DBT, respectively).^{20,21} It is possible to conclude that good to excellent conversions and selectivities, ranging from 90% to 100%, were obtained with the four substrates for all the S/C molar ratios tested (200 and 1000). In this article, by comparing between the ODS performance of different catalysts, the catalytic efficiency of complex 1 is amediocre (Table S5†).

Conclusions

In summary, a new phosphotungstate-supported rhenium carbonyl derivative, [N(CH₃)₄]₆H₄[P₂W₁₇O₆₂{Re(CO)₃]₂·25H₂O, was obtained by using a conventional mixed-solvent solution method. Solution behavior examined *via* ESI-MS showed that complex 1 was stable in CH₃CN medium. In addition, the homogeneous catalytic performance of 1 in the selective oxidation of thiophenes using H₂O₂ as an oxidant in CH₃CN was also demonstrated. The successful isolation of compound 1 provided new scope for obtaining novel POM-based organometallic compounds with intriguing properties. In the following work, we will concentrate on exploring the synthesis of novel structural analogues.

Conflicts of interest

There are no conflicts to declare.

Acknowledgements

We are grateful to the financial support from the National Science Foundation of China (20771034 and 21401042) and the National Key R&D Program of China (2018YFB0605802).

Notes and references

- (a) P. Ma, F. Hu, J. Wang and J. Niu, *Coord. Chem. Rev.*, 2019, **378**, 281–309; (b) D. Li, P. Ma, J. Niu and J. Wang, *Coord. Chem. Rev.*, 2019, **392**, 49–80; (c) L. Cronin and A. Müller, *Chem. Soc. Rev.*, 2012, **41**, 7333–7334; (d) H. N. Miras, J. Yan, D.-L. Long and L. Cronin, *Chem. Soc. Rev.*, 2012, **41**, 7403–7430; (e) H. Lv, Y. V. Geletii, C. Zhao, J. W. Vickers, G. Zhu, Z. Luo, J. Song, T. Lian, D. G. Musaev and C. L. Hill, *Chem. Soc. Rev.*, 2012, **41**, 7572–7589; (f) K. Kamata, K. Yonehara, Y. Nakagawa, K. Uehara and N. Mizuno, *Nat. Chem.*, 2010, **2**, 478–483; (g) A. Proust, B. Matt, R. Villanneau, G. Guillemot, P. Gouzerh and G. Izzet, *Chem. Soc. Rev.*, 2012, **41**, 7605–7622.
- (a) N. Mizuno, D. K. Lyon and R. G. Finke, *J. Catal.*, 1991, **128**, 84–91; (b) N. Mizuno, H. Weiner and R. G. Finke, *J. Mol. Catal. A: Chem.*, 1996, **114**, 15–28; (c) Y. Imada, T. Shido, R. Ohnishi, K. Isobe and M. Ichikawa, *Catal. Lett.*, 1996, **38**, 101–108; (d) J. Lu, X. Ma, V. Singh, Y. Zhang, P. Ma, C. Zhang, J. Niu and J. Wang, *Dalton Trans.*, 2018, **47**, 5279–5285; (e) J. Jia, Y. Niu, P. Zhang, D. Zhang, P. Ma, C. Zhang, J. Niu and J. Wang, *Inorg. Chem.*, 2017, **56**, 10131–10134; (f) J. Li, J. Guo, J. Jia, P. Ma, D. Zhang, J. Niu and J. Wang, *Dalton Trans.*, 2016, **45**, 6726–6731; (g) W. J. Choi and C. Y. Choi, *Biotechnol. Bioprocess Eng.*, 2005, **10**, 167; (h) C. Zhao, W. R. Cordoba, A. L. Kaledin, Y. Yang, Y. V. Geletii, T. Lian, D. G. Musaev and C. L. Hill, *Inorg. Chem.*, 2013, **52**, 13490–13495.
- (a) P. Gouzerh and A. Proust, *Chem. Rev.*, 1998, **98**, 77–112; (b) C. J. Besecker and W. G. Klemperer, *J. Am. Chem. Soc.*, 1980, **102**, 7598–7600; (c) V. W. Day, M. F. Fredrich, M. R. Thompson, W. G. Klemperer, R. S. Liu and W. Shum, *J. Am. Chem. Soc.*, 1981, **103**, 3597–3599; (d) W. G. Klemperer and D. J. Main, *Inorg. Chem.*, 1990, **29**, 2355–2360; (e) W. G. Klemperer and B. X. Zhong, *Inorg. Chem.*, 1993, **32**, 5821–5826; (f) C. Zhao, Z. Huang, W. Rodríguez-Córdoba, C. S. Kambara, K. P. O'Halloran, K. I. Hardcastle, D. G. Musaev, T. Lian and C. L. Hill, *J. Am. Chem. Soc.*, 2011, **133**, 20134–20137.
- (a) T. Nagata, B. M. Pohl, H. Weiner and R. G. Finke, *Inorg. Chem.*, 1997, **36**, 1366–1377; (b) Z.-X. Li, H. Ma, S.-L. Chen, Z.-D. Pan, Y.-F. Zeng, X.-L. Wang and X.-H. Bu, *Dalton Trans.*, 2011, **40**, 31–34.
- (a) J. Niu, L. Yang, J. Zhao, P. Ma and J. Wang, *Dalton Trans.*, 2011, **40**, 8298–8300; (b) D. Zhang, J. Zhao, Y. Zhang, X. Hu, L. Li, P. Ma, J. Wang and J. Niu, *Dalton Trans.*, 2013, **42**, 2696–2699; (c) Z. Huo, J. Guo, J. Lu, Q. Xu, P. Ma, J. Zhao, D. Zhang, J. Niu and J. Wang, *RSC Adv.*, 2015, **5**, 69006–69009; (d) Z. Huo, J. Zhao, Z. Bu, P. Ma, Q. Liu, J. Niu and J. Wang, *ChemCatChem*, 2014, **6**, 3096–3100; (e) J. Lu, X.

- Ma, V. Singh, Y. Zhang, P. Wang, J. Feng, P. Ma, J. Niu and J. Wang, *Inorg. Chem.*, 2018, **57**, 14632–14643; (f) J. Lu, X. Ma, P. Wang, J. Feng, P. Ma, J. Niu and J. Wang, *Dalton Trans.*, 2019, **48**, 628–634.
- 6 (a) R. Martinez-Palou and R. Luque, *Energy Environ. Sci.*, 2014, **7**, 2414–2447; (b) W. S. Zhu, B. L. Dai, P. W. Wu, Y. H. Chao, J. Xiong, S. H. Xun, H. P. Li and H. M. Li, *ACS Sustainable Chem. Eng.*, 2015, **3**, 186–194.
- 7 H. Y. Lü, Y. N. Zhang, Z. X. Jiang and C. Li, *Green Chem.*, 2010, **12**, 1954–1958.
- 8 (a) M. Te, C. Fairbridge and Z. Ring, *Appl. Catal., A*, 2001, **219**, 267–280; (b) J. Xu, S. Zhao, W. Chen, M. Wang and Y.-F. Song, *Chem. – Eur. J.*, 2012, **18**, 4775–4781; (c) D. Julião, R. Valença, J. C. Ribeiro, B. de Castro and S. S. Balula, *Appl. Catal., A*, 2017, **537**, 93–99.
- 9 (a) L. S. Nogueira, S. Ribeiro, C. M. Granadeiro, E. Pereira, G. Feio, L. Cunha-Silva and S. S. Balula, *Dalton Trans.*, 2014, **43**, 9518–9528; (b) S. Ribeiro, A. D. S. Barbosa, A. C. Gomes, M. Pillinger, I. S. Gonçalves, L. Cunha-Silva and S. S. Balula, *Fuel Process. Technol.*, 2013, **116**, 350–357; (c) D. Julião, A. C. Gomes, M. Pillinger, L. Cunha-Silva, B. de Castro, I. S. Gonçalves and S. S. Balula, *Fuel Process. Technol.*, 2015, **131**, 78–86.
- 10 R. Contant, W. G. Klemperer and O. Yaghi, in *Inorganic Syntheses*, John Wiley & Sons, Ltd, 2007, pp. 104–111.
- 11 O. V. Dolomanov, L. J. Bourhis, R. J. Gildea, J. A. K. Howard and H. Puschmann, *J. Appl. Crystallogr.*, 2009, **42**, 339–341.
- 12 (a) G. M. Sheldrick, *Acta Crystallogr., Sect. A: Found. Crystallogr.*, 2008, **64**, 112–122; (b) G. M. Sheldrick, *Acta Crystallogr., Sect. C: Struct. Chem.*, 2015, **71**, 3–8.
- 13 I. D. Brown and D. Altermatt, *Acta Crystallogr., Sect. B: Struct. Sci.*, 1985, **41**, 244–247.
- 14 L. Yang, X. Ma, P. Ma, J. Hua and J. Niu, *Cryst. Growth Des.*, 2013, **13**, 2982–2989.
- 15 (a) R. Villanneau, R. Delmont, A. Proust and P. Gouzerh, *Chem. – Eur. J.*, 2000, **6**, 1184–1192; (b) A. V. Besserguenev, M. H. Dickman and M. T. Pope, *Inorg. Chem.*, 2001, **40**, 2582–2586; (c) R. Villanneau, A. Proust, F. Robert and P. Gouzerh, *Chem. – Eur. J.*, 2003, **9**, 1982–1990.
- 16 (a) Y. W. Li, Y. G. Li, Y. H. Wang, X. J. Feng, Y. Lu and E. B. Wang, *Inorg. Chem.*, 2009, **48**, 6452–6458; (b) P. Zhang, V. Singh, J. Jia, D. Zhang, P. Ma, J. Wang and J. Niu, *Dalton Trans.*, 2018, **47**, 9317–9323.
- 17 (a) S. Chen, P. Ma, H. Luo, Y. Wang, J. Niu and J. Wang, *Chem. Commun.*, 2017, **53**, 3709–3712; (b) U. Warzok, L. K. Mahnke and W. Bensch, *Chem. – Eur. J.*, 2019, **25**, 1405–1419; (c) A. J. Surman, P. J. Robbins, J. Ujma, Q. Zheng, P. E. Barran and L. Cronin, *J. Am. Chem. Soc.*, 2016, **138**, 3824–3830.
- 18 (a) V. Chandra Srivastava, *RSC Adv.*, 2012, **2**, 759–783; (b) K.-E. Jeong, T.-W. Kim, J.-W. Kim, H.-J. Chae, C.-U. Kim, Y.-K. Park and S.-Y. Jeong, *Korean J. Chem. Eng.*, 2013, **30**, 509–517; (c) H. Li, W. Zhu, Y. Wang, J. Zhang, J. Lu and Y. Yan, *Green Chem.*, 2009, **11**, 810–815; (d) H. Mirhoseini and M. Taghdiri, *Fuel*, 2016, **167**, 60–67.
- 19 (a) V. Hulea, P. Moreau and F. Di Renzo, *J. Mol. Catal. A: Chem.*, 1996, **111**, 325–332; (b) V. Hulea, F. Fajula and J. Bousquet, *J. Catal.*, 2001, **198**, 179–186; (c) E. Dumitriu, C. Guimon, A. Cordoneanu, S. Casenave, T. Hulea, C. Chelaru, H. Martinez and V. Hulea, *Catal. Today*, 2001, **66**, 529–534.
- 20 (a) X. Hu, Y. Lu, F. Dai, C. Liu and Y. Liu, *Microporous Mesoporous Mater.*, 2013, **170**, 36–44; (b) X. Wang, L. Xu, X. Chen, W. Ji, Q. Yan and Y. Chen, *J. Mol. Catal. A: Chem.*, 2003, **206**, 261–268; (c) C. Komintarachat and W. Trakarnpruk, *Ind. Eng. Chem. Res.*, 2006, **45**, 1853–1856.
- 21 Y. Niu, Q. Xu, Y. Wang, Z. Li, J. Lu, P. Ma, C. Zhang, J. Niu and J. Wang, *Dalton Trans.*, 2018, **47**, 9677–9684.